Prediction of stall inception in an axial flow compressor†

K. L. Lewis*

(Received October 1990)

The small perturbation stability analysis of Nenni and Ludwig [1] to predict stall inception of a high hub-to-tip ratio blade row was extended by establishing the blade row compatibility equations in the relative frame of reference and applying them to a diffusing control volume. This control volume represents a simplified form of the flow passage found between two blades in a compressor rotor or stator. The model predicts a neutral stability point at which a disturbance is neither amplified nor damped, as well as the frequency of the resulting disturbance. The model was applied to a rotor in a single stage environment for which extensive experimental data was available. The correlation of experimental and model results was acceptable. Stall inception was predicted in terms of stalling inlet angle to within 0,5 degrees in the tip region. The corresponding disturbance velocity was predicted as 0,56 blade speed compared to the measured value of 0,62 for the complete annulus. The predictive capability of the model was found to be very sensitive to the blade row performance characteristic. A parametric study was performed to study the influence of the area ratio of the diffusing control volume. It was found that an increase in area ratio of the diffusing passage tended to delay stall inception but decrease the disturbance velocity.

List of symbols

A	area	[m²]
c	chord	[m]
f	frictional forces	[N/kg]
G	function relating blade exit angle to inlet angle	
H	total specific enthalpy	[J/kg]
h	specific enthalpy	[J/kg]
j	imaginary number	
L	effective length	[m]
n	wave number	
p	pressure	[N/m²]
r	radius	[m]
R	area ratio	
S	tangent of swirl angle	
t	time	[s]
v	absolute velocity	[m/s]
w	relative velocity	[m/s]
z	axial coordinate	[m]
β	relative angle	[degree]
η	vorticity	[1/s]
Λ	eigen-value	
ω	angular velocity	[rad/s]
ϕ	disturbance function, flow coefficient	
ρ	density	[kg/m³]
σ	complex number, solidity	
ζ	total pressure loss coefficient	
θ	circumferential angle coordinate	

subscripts		superscripts	
0	total	′	differential
1	inlet	^	perturbation
2	exit	–	mean
b	blade	~	Fourier coefficient
cv	control volume	→	vector
p	disturbance		

QS	quasi-steady
R	relative
r	radial
ref	reference
SS	steady state
s	stalling
z	axial
θ	circumferential

†This paper is based on a MSc thesis submitted by the author to the School of Mechanical Engineering, University of the Witwatersrand.

*Engineer
Bureau for Mechanical Engineering
University of Stellenbosch

1. Introduction

The position of the stall line is a matter of great concern to the compressor designer as it generally represents a limit to the useful operation of the compressor. Crossing this line can result in large performance penalties, severe vibratory stressing of the blades and initiation of surge.

The prediction of stall has been attempted at several quite different levels of approach. These include empirical correlations, linearized stability analyses, non-linear investigations of rotating stall onset and growth, and multi-element stability models. Greitzer [2] reviews all of these methods; only linearized techniques are considered in this paper.

Emmons et al [3] were the first to perform a linearized stability analysis by investigating the conditions under which a small amplitude circumferentially non-uniform, two-dimensional flow perturbation in a cascade would grow and therefore indicate the onset of rotating stall. Since then there have been many extensions of the perturbation analysis of which recent examples are the papers by Dunham [4], Ferrand and Chauvin [5] and Takata and Nagashima [6]. All methods use an actuator or semi-actuator disc representation of the blade row. This implicitly assumes that the detailed flow conditions within the blade passage do not directly produce or inhibit stall. Evidence suggests that this is acceptable as long as the model is used to predict stall inception only.

This paper presents an extension of the small perturbation analysis of Nenni and Ludwig [1]. An improved representation of the blade row is included in the form of a semi-actuator disc of finite thickness which accounts for blade geometry by the consideration of a one-dimensional diffuser blade passage. The model is contained in

section 2 whilst section 3 presents the experimental data necessary for the evaluation of the model. In section 4 the results of the model predictions are discussed.

2. Mathematical Model

The use of perturbation methods in problems of hydrodynamic stability is suggested by the concept that a steady flow field is stable if no unsteady disturbance of it grows with time. The model comprises an analysis of the intra blade row flow field with the resulting constants of integration being evaluated by the boundary conditions. It is required that the only destabilizing phenomenon is derived from the steady flow field itself.

2.1 Analysis of flow field in blade-free zone

The flow in the blade-free zone is assumed to be incompressible and inviscid; the incompressible formulation of the Euler equations are therefore valid in describing this flow together with the unsteady continuity equation

$$\frac{\partial \vec{v}}{\partial t} + (\vec{v}.\nabla)\,\vec{v} = -\frac{1}{\rho}\,\nabla p \qquad 2.1$$

$$\nabla.\vec{v} = 0 \qquad 2.2$$

The unsteady flow model assumes that superimposed on a steady fully specified flow field is an unknown velocity and pressure perturbation such that

$$\vec{v} = \bar{\vec{v}} + \hat{\vec{v}} \qquad 2.3$$

$$p = \bar{p} + \hat{p} \qquad 2.4$$

By assuming that the amplitude of the perturbations remain small the momentum and continuity equations can be formulated explicitly in the perturbation quantities and can be linearized by neglecting second order terms. By assuming that the flow is cylindrical and that the steady-flow field is axisymmetric results in the following equations

$$\frac{\partial \hat{v}_\theta}{\partial t} + \frac{\bar{v}_\theta}{r}\frac{\partial \hat{v}_\theta}{\partial \theta} + \bar{v}_z\frac{\partial \hat{v}_\theta}{\partial_z} = -\frac{1}{r\bar{\rho}}\frac{\partial \hat{p}}{\partial \theta} \qquad 2.5$$

$$\frac{\partial \hat{v}_z}{\partial t} + \frac{\bar{v}_\theta}{r}\frac{\partial \hat{v}_z}{\partial \theta} + \bar{v}_z\frac{\partial \hat{v}_z}{\partial_z} = -\frac{1}{\bar{\rho}}\frac{\partial \hat{p}}{\partial z} \qquad 2.6$$

$$\frac{1}{r}\frac{\partial \hat{v}_\theta}{\partial \theta} + \frac{\partial \hat{v}_z}{\partial_z} = 0 \qquad 2.7$$

To obtain an analytical solution it is assumed that the perturbations are periodic in time and the θ – direction. Then for each blade-free region the perturbation quantities can be given in the form of a Fourier series

$$\hat{v}_\theta = \sum_{n=1}^{\infty} \tilde{v}_{\theta,n}(z)\, e^{j(\sigma t + n\theta)}$$

$$\hat{v}_z = \sum_{n=1}^{\infty} \tilde{v}_{z,n}(z)\, e^{j(\sigma t + n\theta)}$$

$$\hat{p} = \sum_{n=1}^{\infty} \tilde{p}_n(z)\, e^{j(\sigma t + n\theta)} \qquad 2.8$$

Substitution of these Fourier series into equations 2.5-2.7 and by defining a disturbance stream function ϕ such that

$$\hat{\phi} = \sum_{n=1}^{\infty} \tilde{\phi}_n(z)\, e^{j(\sigma t + n\theta)}$$

$$\tilde{v}_{z,n} = -j\frac{n}{r}\tilde{\phi}_n$$

$$\tilde{v}_{\theta,n} = \frac{d\tilde{\phi}_n}{dz} \qquad 2.9$$

and eliminating $\tilde{p}_n$ leads to the basic two-dimensional small-perturbation equation of unsteady flow in the blade-free zone for the n^{th} harmonic

$$\left(\bar{v}_z\frac{d}{dz} + j\left(\sigma + \frac{n}{r}\bar{v}_\theta\right)\right).\left(\frac{d^2\tilde{\phi}_n}{dz^2} - \frac{n^2\tilde{\phi}_n}{r^2}\right) = 0 \qquad 2.10$$

This is a linear third order equation; solving for the three roots and the velocity perturbations described by equation 2.9 and transforming these to the relative coordinate system results in the following expressions for the perturbations

$$\hat{w}_z = \sum_{n=1}^{\infty}\left(A_n e^{\frac{nz}{r}} + B_n e^{\frac{-nz}{r}} + D_n e^{-j\left(\frac{nz}{r}\right)(\Lambda+S_R)}\right).e^{j((\sigma+\omega)t+n\theta)}$$

$$\hat{w}_\theta = \sum_{n=1}^{\infty}\Big(jA_n e^{\frac{nz}{r}} - jB_n e^{\frac{-nz}{r}} + (\Lambda+S_R)\,D_n e^{-j\left(\frac{nz}{r}\right)(\Lambda+S_R)}\Big).e^{j((\sigma+\omega)t+n\theta)}$$

$$\hat{p} = -\rho\bar{w}_z\sum_{n=1}^{\infty}\left(\left(1 + j(\Lambda + S_R)\frac{\omega r}{\bar{w}_z}\right)A_n e^{\frac{nz}{r}} + (1 - j(\Lambda + S_R))\left(B_n e^{\frac{-nz}{r}}\right)\right).e^{j((\sigma+n\omega)t+n\theta)}$$

where $\Lambda = \dfrac{\sigma r}{n\bar{w}_z} + \dfrac{\omega r}{\bar{w}_z}$ 2.11

where A_n, B_n and D_n are the coefficients of integration for the n^{th} harmonic and S_R is the tangent of the steady relative swirl angle.

Equations 2.11 completely define the small perturbation unsteady flow field in the blade-free zone and only the three constants of integration require solution; these are determined by the boundary conditions.

2.2 Boundary Conditions

There are two types of boundary condition; those which relate to conditions far upstream and far downstream and those which pertain to boundaries formed by the blade rows.

Far upstream of the blade row the unsteady flow is required to diminish to zero. This is commensurate with the assumption that there is no external forcing function that precipitates flow field instability; it is the steady flow field itself that induces rotating stall. Downstream of the blade row it is required that the velocity amplitudes remain at least finite. These two conditions are satisfied if

$$B_{n,1} = A_{n,2} = 0$$

where the subscripts 1 and 2 refer to upstream and downstream of the blade row respectively.

Again upstream of the first blade row the flow everywhere is assumed to be irrotational by virtue of Helmholtz's vorticity theorem. Defining the r-component of vorticity as

$$\hat{\eta}_r = \frac{1}{r}\frac{\partial \hat{w}_z}{\partial \theta} - \frac{\partial \hat{w}_\theta}{\partial z} \qquad 2.12$$

the condition of upstream irrotationality implies

$$D_{n,1} = 0$$

2.3 *Blade row representation*

Having defined the unsteady flow in the blade-free regions, a mathematical model is necessary to match the flow conditions immediately upstream of the blade row to those conditions downstream, these matching conditions embodying the assumed blade row aerodynamics.

Three equations per blade row are necessary to determine the constants of integration defined in the general unsteady flow solution for the blade-free regions. The matching conditions used are conservation of mass flow, conservation of rothalpy and vorticity, and a flow deflection relation.

Since the perturbation flow is assumed incompressible the conservation of mass flow through the actuator requires that the axial velocity is continuous across the blade row.

$$\hat{w}_{z,1} = \hat{w}_{z,2} \qquad 2.13$$

This boundary condition does not take into account the relative circumferential displacement of the flow between inlet and exit of the blade row due to blade stagger; this is not expected to influence the predictive capability of the model.

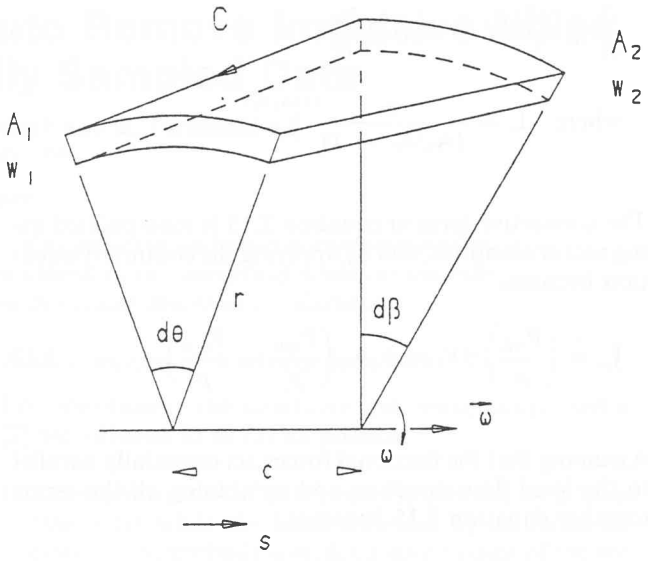

Figure 1 – Semi-actuator blade passage representation

The second boundary condition is evaluated by the consideration of the conservation of vorticity and is essentially an extension of Helmholtz's vorticity law to consider flow with losses.

It can be shown that the circulation around a closed contour can be described by the following equation

$$\frac{\partial \Gamma_R}{\partial t} - \oint_c d\vec{r}_R . (\vec{w} \times \vec{\eta}) = \oint_c d\vec{r}_R . (2\vec{w} \times \vec{\omega} + \vec{f}) \qquad 2.14$$

where the closed contour C is shown in figure 1. This equation essentially states that an irrotational incompressible flow may be changed into a rotational motion by the effect of frictional forces.

This equation is strictly applicable to a flow model in which the blade rows are present. For the present type of flow model where an actual blade row is replaced by a cascade containing an infinite number of infinitely thin blades, the actions of the blades must be replaced by the effects of extraneous forces. However, as the line integral around the closed contour C is taken, only the loss producing or non-conservative forces need to be considered; the line integral of a conservative force such as that produced by blade lift is zero.

In order to utilize the vorticity compatibility relation, an expression relating the loss producing forces to the conservation of rothalpy is required. Since the flow geometry is axisymmetric the conservation of relative total pressure can replace that of rothalpy. Use is made of the unsteady relative energy equation which is integrated about the control volume in figure 1 which gives

$$\frac{\partial}{\partial t}\int_{cv} \frac{w^2}{2}\, dV + \int_{cv} \vec{w} . \nabla \left(\frac{P_{OR}}{\rho}\right) dV = \int_{cv} \vec{w} . \vec{f}\, dV \qquad 2.15$$

The flow through the actuator disc is assumed incompressible and the flow area A, a function of the steady flow field only. If the area of the control volume is assumed to vary linearly the first term in equation 2.15 is given by

$$\frac{\partial}{\partial t}\int_{cv}\frac{w^2}{2}\,dV = w_1 A_1 L\frac{\partial \hat{w}_1}{\partial t} \qquad 2.16$$

where $L = \dfrac{c}{(A_2/A_1 - 1)^{\ln (A_2/A_1)}}$

The convective term in equation 2.15 is manipulated using vector identities, and by applying the continuity equation becomes

$$\int_{cv}\vec{w}.\left(\frac{P_{OR}}{\rho}\right)dV = \bar{w}_1 A_1\left(\frac{P_{02R}}{\rho} - \frac{P_{01R}}{\rho}\right) \qquad 2.17$$

Assuming that the frictional forces act essentially parallel to the local flow direction and combining all the terms together equation 2.15 becomes

$$L\frac{\partial \hat{w}_1}{\partial t} + \left(\frac{P_{02R}}{\rho} - \frac{P_{01R}}{\rho}\right) = \int_1^2 \vec{ds}.\vec{f} \qquad 2.18$$

The left hand side of equation 2.18 is by definition related to the unsteady total pressure loss coefficient ζ such that

$$\zeta = \frac{\dfrac{P_{01R}}{\rho} - \dfrac{P_{02R}}{\rho} - L\dfrac{\partial \hat{w}_1}{\partial t}}{\frac{1}{2}\bar{w}_1^2} \qquad 2.19$$

It is assumed that the unsteady coefficient may be approximated by the addition of the unsteady inertia term to the steady loss. The steady loss coefficient is treated in a quasi-steady manner by applying a Taylor series expansion

$$\zeta = \zeta\left(\tan\beta_1, \frac{\partial \hat{w}_1}{\partial t}\right) = \zeta(\tan\bar{\beta}_1) + \frac{d\zeta(\tan\bar{\beta}_1)}{d\tan\bar{\beta}_1}.\delta(\tan\beta_1) - \frac{2L}{\bar{w}_1^2}\frac{\partial \hat{w}_1}{\partial t} \qquad 2.20$$

By applying the binomial expansion the unsteady perturbation $\delta(\tan\beta_1)$ is given by

$$\delta(\tan\beta_1) = \frac{\hat{w}_{\theta,1} - \hat{w}_{z,1}\tan\bar{\beta}_1}{\bar{w}_z} \qquad 2.21$$

Sufficient information is now available to apply the vorticity equation to the closed contour C. As the number of blades approaches infinity the following is obtained

$$\frac{\partial}{\partial t}(R\,\hat{w}_{\theta,2} - \hat{w}_{\theta,1}) - \bar{w}_z(R\hat{\eta}_{r,2} - \hat{\eta}_{r,1}) - \frac{L}{r}\sec\beta_1\frac{\partial^2 \hat{w}_{z,1}}{\partial\theta\partial t} = \frac{w_z}{r}\left(\left(S_{R,1}\zeta + (1+S_{R,1}^2)\frac{\zeta'}{2}\right)\frac{\partial \hat{w}_{\theta,1}}{\partial\theta} + \left(\zeta - S_{R,1}^2(1+S_{R,1}^2)\frac{\zeta'}{2}\right).\frac{\partial \hat{w}_{z,1}}{\partial\theta}\right) \qquad 2.22$$

where $R = A_2/A_1$

The final boundary condition supplies a relation between the blade exit angle in terms of blade inlet angle. Using a similar approach to that represented in equation 2.20, the following is obtained

$$\hat{w}_{\theta,2} - S_{R,2}\,\hat{w}_{z,2} - \bar{G}'.(\hat{w}_{\theta,1} - S_{R,1}\,\hat{w}_{z,1}) \qquad 2.23$$

where $\bar{G}' = \dfrac{d\bar{G}(\tan\bar{\beta}_1)}{d\tan\bar{\beta}_1}$

The boundary conditions that have been derived are linear in terms of the perturbation velocities. This means that the Fourier components can be defined directly.

These conditions formulate the blade row characteristic equations relating the unsteady flow conditions upstream and downstream of each blade row. It is now possible to mathematically determine specific values for the constants of integration which appear in the general unsteady flow solution for the regions upstream and downstream of the blade row. Therefore for each harmonic n, a set of blade row boundary conditions is generated which contributes to the corresponding set of constants of integration. Substitution of the general unsteady flow solution into the Fourier constituents of the blade row boundary equations yields a system of homogeneous equations for the unknowns $A_{n,1}$, $B_{n,2}$ and $D_{n,2}$.

To obtain a non-trivial solution the eigen-value Λ of the system is evaluated. This is derived from the determinant of the system

$$\begin{vmatrix} 1 & -1 & -1 \\ -j\Lambda k_1 - k_2(1 + jS_{R,1}) & -j\Lambda R & -R(1 + S_{R,2}(S_{R,2} + \Lambda)) \\ \bar{G}'(1 + jS_{R,1}) & 1 - jS_{R,2} & j\Lambda \end{vmatrix} = 0 \qquad 2.24$$

where

$$K_1 = 1 + \frac{Ln}{r}\sec\bar{\beta}_1$$

$$k_2 = \bar{\zeta} + \frac{j}{2}\bar{\zeta}'(1 + S_{R,1}^2)$$

The first root is the zero amplitude solution

$$\Lambda_1 = -(S_{R,2} + j) \qquad 2.25$$

This solution predicts instability throughout the operating range and represents a singularity in the downstream flow conditions. Substitution of this root into the simultaneous equations entails the removal of the rotational flow term which always results in the determinant being zero. The trivial solution needs to be factored out of the quadratic equation in order for the other root to be ob-

tained. Other workers including Nenni and Ludwig [1] obtained the same root.

The second root consists of real and imaginary components

$$\Lambda_2 = \frac{\text{Real}\,(\sigma)\,r}{n\bar{w}_z} + \frac{\text{Imag}\,(\sigma)\,r}{n\bar{w}_z}$$

$$= -\frac{1}{1 + R + \frac{Ln}{r}\sec\bar{\beta}_1}\left(\bar{G}'R(S_{R,2} + S_{R,1})\right.$$

$$\left. + S_{R,1}\bar{\zeta} + \frac{\bar{\zeta}'}{2}(1 + S^2_{R,1})\right) +$$

$$\frac{j}{1 + R + \frac{Ln}{r}\sec\bar{\beta}_1}\left(\bar{G}'R(1 - S_{R,1}S_{R,2})\right.$$

$$\left. + R(1 + S^2_{R,2}) + \bar{\zeta} - \frac{S_{R,1}}{2}\bar{\zeta}'(1 + S^2_{R,1})\right) \qquad 2.26$$

Stall inception occurs when the imaginary part of the root passes through zero and becomes negative. There is no direct reference in the stall inception limit expression to the blade row characteristics other than the blade loss and turning relationships, and overall area ratio; although the blade chord c which is incorporated in L features in the eigen-value matrix it is only included in the real and imaginary components of σ as part of a multiplier. It does not influence the point at which the damping factor passes through zero. From this it can be inferred that although it has been found by experiment that an increase in chord length improves the stall limit of a blade row, it does so in an indirect manner via the blade loss and turning characteristics.

The real part of the non-trivial root gives the propagation velocity of the disturbance as a fraction of the axial velocity. The propagation velocity becomes

$$\frac{v_p}{v_b} = \frac{r}{n}\left(1 + \frac{\bar{w}_z}{v_b}\left(\frac{\text{Real}\,(\sigma)\,r}{\bar{w}_z}\right)\right) \qquad 2.27$$

3. Experimental Data

Extensive experimental data was obtained by the author on a low speed axial flow compressor and is reported in [7]. A single stage configuration was used with the stator positioned five chord lengths downstream from the rotor. This position was chosen such that there would be minimal coupling between the stator and rotor flow fields and therefore allow the rotor to be tested as a single blade row but in a single stage environment. The compressor blading was based on an 80% reaction design using NACA 65 profiles on a circular arc camber line. No inlet guide vanes were necesasary due to the high reaction. The rotor blade-chord Reynolds number at design point was $1{,}3 \times 10^5$. The hub-to-tip ratio was 0,714.

Blade row performance was determined by traversing at inlet and exit from the rotor with a three hole probe. Characteristics as shown in figure 2 and 3 were obtained for the hub, midspan and tip regions by mass averaging the respective data. Similar data were obtained for the complete annulus. Kulite pressure transducers mounted on the casing wall were used to determine the number of stall cells and their frequency.

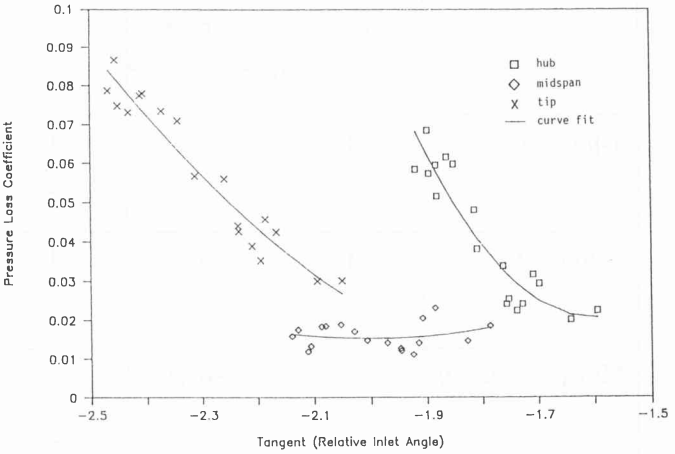

Figure 2 – Mass averaged hub, midspan and tip characteristics of pressure loss

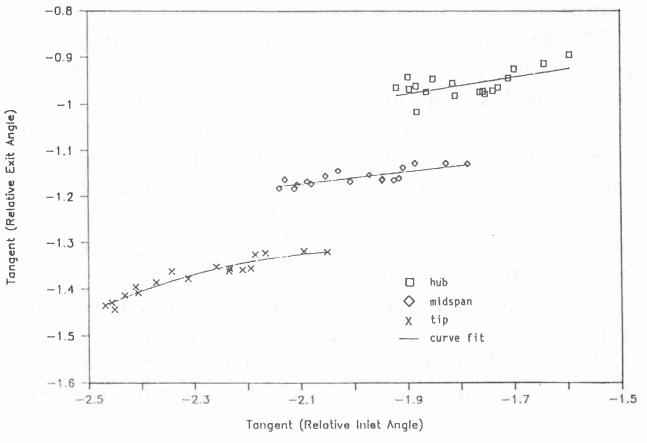

Figure 3 – Mass averaged hub, midspan and tip characteristics of flow turning

4. Application of Stability Model

The stability criterion defines the limit at which a streamtube through a blade row is transformed from a steady stable flow to one that is stable only in an unsteady mode. The streamtube is defined as being thin and annular and containing a blade row with predetermined steady characteristics.

The analysis can be applied in two ways. Firstly the stability of a streamtube which encompasses the whole blade span can be determined if a two-dimensional representation of the flow approximates the actual situation.

Table 1: Comparison of Predicted and Measured Stall Inception Data

	PREDICTED				EXPERIMENTAL		
Stream Tube (% Blade Span)	Area Ratio R	Stall Angle β_{1s}	Wave Number n	Disturbance Velocity v_p/v_b	Angle at stall β_1	Wave Number n	Cell Velocity v_p/v_b
Total (8-92)	1	−67,3	1	0,55	−65,2	3	0,62
			2	0,61			
			3	0,66			
	1,44	−68,4	1	0,46			
			2	0,53			
			3	0,58			
Tip (70-92)	1	−68,4	1	0,40	−68,0		
			2	0,44			
			3	0,56			
Hub (8-30)	1	−63,7	1	0,67	−62,5		
			2	0,71			
			3	0,72			
Midspan (30-70)	1	−69,5	1	0,68	−65,0		
			2	0,73			
			3	0,77			

The latter is approximately true in a high hub-to-tip ratio compressor.

The second approach is to consider streamtubes that occupy only a certain fraction of the blade row annulus. Again the flow is assumed to be two-dimensional and the objective of the analysis is to determine which streamtubes will become unstable first. If the flow is identified as unstable in one or more streamtubes but stable in others, full rotating stall will only develop if there is insufficient damping across the whole blade row. This is determined by the former approach.

The curve-fitted blade row characteristics shown in figures 2 and 3 were used as input to the inception model, in addition to the respective mean axial velocities and blade geometry parameters. The model was then used to determine the neutral stability point represented by the transition of the stability parameter through zero as well as the corresponding disturbance velocity. As the model does not predict the number of disturbances or stall cells, the wave number becomes another input. A summary of the stall inception points as predicted by the model are compared to the experimental data in table 1.

The influence of the area ratio R is seen to delay stall inception; if R is chosen to be unity, that is the blade passage is parallel-sided, a stalling inlet angle β_{1s} of −67,3 degrees is predicted for the complete annulus. Increasing the value of R to the geometric value of 1,44 delays stall inception with β_{1s} equaling −68,4 degrees. As a better correlation was obtained for R = 1, this was retained throughout the rest of the analysis.

The influence of wave number n is seen to affect only the disturbance velocity v_p/v_b; the wave number was varied from the inception value of a single cell to the steady fully developed value of three. Figure 4 and 5 show the graphical results of varying R and n.

If these results are compared to the experimental ones reasonable correlation exists; however it can be seen that actual stalling occurs earlier than that predicted. There are two possible reasons for this discrepancy; either the model is invalid in the assumptions taken or the experimental data used as input is not representative. It was found that the model, as can be expected, is extremely sensitive to the gradient of the blade row characteristics. As only a second order polynomial could be justified in curve-fitting the pressure loss data whilst a straight line was used to correlate the blade deflection data it is thought that improving these would improve the degree

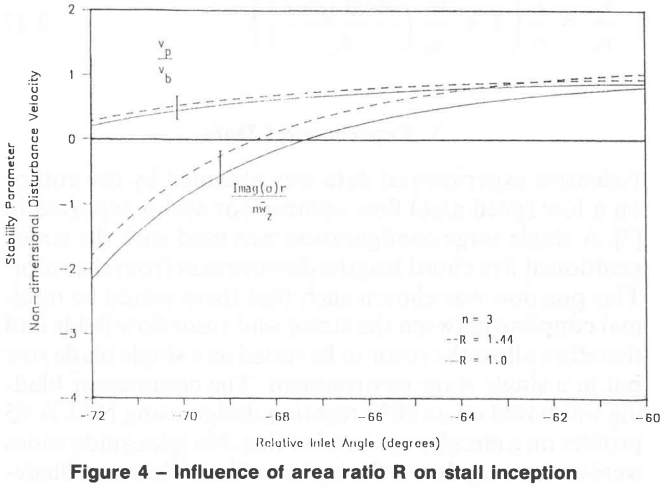

Figure 4 – Influence of area ratio R on stall inception

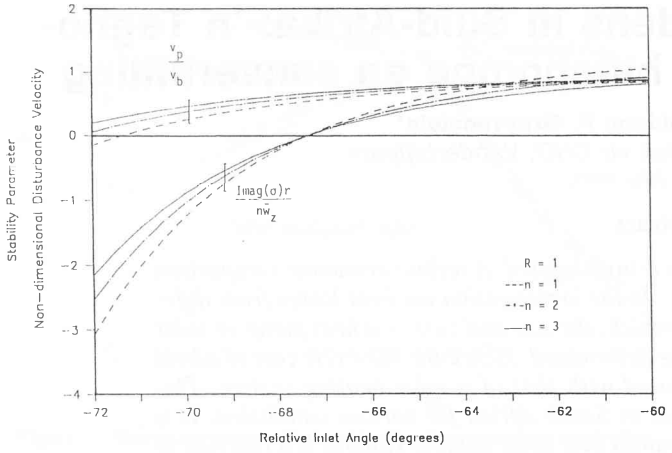

Figure 5 – Influence of wave number n on stall inception

of correlation between the predicted and experimental points.

When the data was applied to the hub, midspan and tip regions a far better correlation was obtained; the model predicted that the tip would stall first at an inlet angle β_{1s} equal to $-68{,}4$ degrees. This is 0,4 degrees from the measured inception point. The fact that the rotor first experienced tip stalling was confirmed by experiment. If the diffusion factors are compared at tip, hub and midspan as in table 2, it would be erroneous to believe that as the hub has the highest value it would stall first. It is however interesting to note that the rule of thumb stating that a diffusion factor greater than 0,6 leads to stall, is generally valid here.

Table 2: Diffusion Factors at Hub, Midspan and Tip ($\phi = 0{,}47$)

Blade Position (% Blade span)	Exit Velocity $\bar{W}_2$ (m/s)	Inlet Velocity $\bar{w}_1$ (m/s)	Exit Angle β_2 90°	Inlet Angle β_1 90°	Solidity σ	Diffusion Factor D
8	32,2	55,7	−40,0	−62,0	1,305	0,62
50	43,8	62,5	−49,0	−65,0	1,088	0,55
92	43,2	69,3	−64,1	−68,9	0,8322	0,60

In physical terms the fact that the model predicts that the blade row will stall first at the tip but the complete annulus will only stall later suggests that there is sufficient damping in the rest of the annulus in the hub and midspan regions to absorb the partial stalling of the tip. This was not confirmed by experimental data; the stall experienced is a full span stall covering the whole blade. This discrepancy can be explained by either of two reasons; firstly the accuracy of the curve-fitted data limits the predictive capability of the model or substantial interaction between the tip and midspan regions after tip stalling has occurred leads to significant flow curvature and radial velocities. This would tend to invalidate the two-dimensional model. It is probably a combination of the two that contributes to the observed discrepancy.

Conclusions

The small perturbation analysis of Nenni and Ludwig to predict stall inception of a high hub-to-tip ratio blade row has been extended by improving the representation of the blade row. The agreement of the model predictions with experimental data is reasonable considering the simplicity of the model and the accuracy of the curve-fitted blade row characteristics. The application of this model to other experimental data would be of benefit in gaining experience of the predictive capability of the model as well as identifying any inconsistencies in the assumptions.

Acknowledgements

This work was submitted in the form of a project report to the University of Witwatersrand as partial fulfilment towards a MSc (Eng) degree. The experimental work was done in the Fluid Machinery Laboratory of the University of Stellenbosch.

References

1. Nenni, J. P. and Ludwig, R. L., "A theory to predict the inception of rotating stall in axial flow compressors", AIAA Paper AIAA-74-528.
2. Greitzer, E. M., "Review – axial compressor stall", Trans ASME, Jnl Fluids Eng, 1980, *102*, pp. 134-151.
3. Emmons, H. W., Pearson, C. E. and Grant, H. P., "Compressor surge and stall propagation", Trans ASME, 1955, *77*, pp. 455-469.
4. Dunham, J., "Non-axisymmetric flows in axial flow compressors", Mech. Eng. Sc. Monograph No. 3, Inst. Mech. Eng., 1965.
5. Ferrand, P. and Chauvin, J., "Theoretical study of flow instabilities and inlet distortions in axial flow compressors", Trans ASME, Jnl. Eng. Power, 1982, *104*, pp. 715-721.
6. Takata, H. and Nagashima, T., "Rotating stall in three-dimensional blade rows subjected to spanwise shear flow", Seventh International Symposium on Air Breathing Engines, Beijing, China, 1985.
7. Lewis, K. L., "The prediction of stall inception in an axial flow compressor," Msc Project Report, University of Witwatersrand, 1989.